Higher-order interaction induced chimeralike state in a bipartite network

Rumi Kar,[1] V. K. Chandrasekar,[2,*] and D. V. Senthilkumar[1,†]

[1]*School of Physics, Indian Institute of Science Education and Research, Thiruvananthapuram-695551, Kerala, India*

[2]*Department of Physics, Centre for Nonlinear Science & Engineering, School of Electrical & Electronics Engineering, SASTRA Deemed University, Thanjavur-613401, Tamil Nadu, India*

(Received 30 April 2024; accepted 1 August 2024; published 10 September 2024)

We report higher-order coupling induced stable chimeralike state in a bipartite network of coupled phase oscillators without any time-delay in the coupling. We show that the higher-order interaction breaks the symmetry of the homogeneous synchronized state to facilitate the manifestation of symmetry breaking chimeralike state. In particular, such symmetry breaking manifests only when the pairwise interaction is attractive and higher-order interaction is repulsive, and vice versa. Further, we also demonstrate the increased degree of heterogeneity promotes homogeneous symmetric states in the phase diagram by suppressing the asymmetric chimeralike state. We deduce the low-dimensional evolution equations for the macroscopic order parameters using Ott-Antonsen ansatz and obtain the bifurcation curves from them using the software XPPAUT, which agrees very well with the simulation results. We also deduce the analytical stability conditions for the incoherent state, in-phase and out-of-phase synchronized states, which match with the bifurcation curves.

DOI: 10.1103/PhysRevE.110.034205

I. INTRODUCTION

The chimera state is an intriguing collective phenomenon observed in an ensemble of identical nonlinear dynamical systems characterized by regular and complex topological structures. In the nonlinear dynamics literature, the coexisting synchronized and asynchronized domains of oscillators constituting an ensemble is referred to as a chimera state. Such an emerging phenomenon was initially reported in a network of nonlocally coupled phase oscillators [1]. Eventually, distinct chimera states have also been identified across various coupling configurations including local [2,3] and global [4–6] coupling configurations. Furthermore, chimera states have been documented in a wide variety of dynamical systems spreading across distinct disciplines including chemical [7–10], optical [11,12], mechanical [13–15], electrical [16], neuronal networks [17–22], and other domains [23–25]. Theoretical investigations on chimera states encompass various mathematical frameworks [26–28]. Notably, the Ott-Antonsen approach [29] is one of the most frequently employed mathematical frameworks to theoretically deduce their existence conditions and accompanied bifurcation curves involving a large network of phase oscillators. Remarkably, experimental observations of the chimera state have also been reported in distinct disciplines [30,31] after decades of theoretical exploration of the paradigm of chimera.

Initial investigations on chimera states are primarily centered only around nonlocally coupled phase oscillators with closed end boundary conditions, that is, ring configurations [32]. As in-depth investigations on chimera states have evolved along with its potential applications in a plethora of real-world systems [33], this intriguing phenomenon has been explored across diverse network structures including complex networks [34], multilayer networks [35–38], two- and three-dimensional architectures [39–43], and hierarchical layouts [44–47]. Among the complex interactions observed in real-world systems, the bipartite network emerges as a prominent structure in complex network systems providing another avenue for investigating various self-organizing collective patterns. In this configuration, nodes from one group exclusively interact only with nodes from a different group without any intragroup interactions. Such a topological structure has been identified in various networks such as author's collaboration network [48], club member activities network [49], investor-company network [50], and so on. Notably, chimera states have also been reported in bipartite networks [51,52]. In particular, Punetha *et al.* [51] demonstrated that chimera state can manifest in a bipartite network only in the presence of time delay in the interaction among the phase oscillators. However, later investigations revealed chimera states in bipartite network with nonlocal coupling [52,53]. Specifically, in-phase chimera, antiphase chimera, and syn-desyn chimera states are reported in nonlocally coupled phase oscillators [53] and in nonlocally coupled FitzHugh-Nagumo oscillators [52].

For a long time, chimera and chimeralike states are reported in network configurations that are limited to feature only pairwise interactions [15,28,45,54–59]. Nevertheless, the collective dynamics of many real-world systems are influenced not just by pairwise interactions but also by multicomponent interactions, commonly facilitated through simplicial complexes, known as higher-order interactions [60]. Various practical scenarios that exemplify this include coauthorship graphs in science [61], structural [62], and functional [63] brain networks, as well as protein interaction networks [64]. Such network structures cannot be adequately described solely through pairwise interactions; higher-order interactions are essential for a comprehensive understanding.

*Contact author: chandru25nld@gmail.com

†Contact author: skumar@iisertvm.ac.in

Notably, higher-order interactions are shown to play a crucial role in facilitating the self-organizing collective dynamics of networks of coupled oscillators. For instance, inclusion of higher-order interactions results in phenomena such as explosive synchronization [65] and abrupt synchronization, accompanied by multistability [66], which are otherwise not observed purely with pairwise interactions. The phase lag parameter usually plays a significant role in the manifestation of chimera states in networks of phase oscillators [67]. However, recently, it has been shown that higher-order interactions can induce chimera states even in the absence of phase lag parameter [68]. Further, recent investigations have employed higher-order interactions in understanding its impact on the chimera states in various network configurations [69–71].

In this work, we report the phenomenon of higher-order (triad) interaction induced stable chimeralike state in a bipartite network of coupled phase oscillators. We establish the transition from synchronized state to chimeralike state using the numerically estimated macroscopic order parameters. In particular, when the pairwise interaction is an attractive coupling, the bipartite network exhibits transition from in-phase synchronized (symmetric) state to symmetry-breaking chimeralike state as a function of repulsive higher-order interaction. In contrast, when the pairwise interaction is a repulsive coupling, the bipartite network exhibits transition from out-of-phase synchronized (symmetric) state to symmetry-breaking chimeralike state as a function of attractive higher-order interaction. Otherwise, in-phase (out-of-phase) synchronized state is observed for attractive (repulsive) higher-order interaction for attractive (repulsive) pairwise coupling, which will be evident in the two-parameter phase diagrams. The symmetric state is characterized by the macroscopic order parameters $r_1 = r_2$ of both populations, while the symmetry-breaking state is characterized by $r_1 \neq r_2$. The symmetric synchronized states lose their stability via a pitchfork bifurcation leading to a symmetry-breaking chimeralike state. A saddle-node bifurcation gives rise to symmetric synchronized states at large magnitudes of higher-order interaction, which coexists with the chimeralike states. In addition, we show that increase in the degree of heterogeneity of the phase oscillators, in terms of frequency distribution of the phase oscillators, promotes the homogeneous (symmetric) dynamical state in a large region of the parameter space. We also deduce the low-dimensional evolution equations for the macroscopic order parameters using the Ott-Antonsen ansatz and show that the bifurcation curves obtained from them using the XPPAUT software match very well with the simulation boundaries. Furthermore, we also deduce the analytical stability conditions for incoherent state, in-phase, and out-of-phase synchronized states via a linear stability analysis about appropriate equilibrium points, which exactly match with the bifurcation curves obtained using the XPPAUT software.

The plan of the paper is as follows. In Sec. II, we introduce the model of a bipartite network of phase oscillators with both pairwise and higher-order interaction. We deduce the low-dimensional evolution equations for the macroscopic order parameters using the Ott-Antonsen ansatz in Sec. III. We demonstrate our findings in Sec. IV. Finally, we provide our summary and conclusion in Sec. V.

II. BIPARTITE NETWORK

We consider a bipartite network with two populations, each containing N phase oscillators. θ_k^σ represents phase of kth oscillator in the population σ. The governing evolution equation for the kth oscillator is represented as

$$\dot{\theta}_k^\sigma = \omega_k^\sigma + \frac{A}{N_{\sigma'}} \sum_{j=1}^{N_{\sigma'}} \sin\left(\theta_j^{\sigma'} - \theta_k^\sigma\right) + \frac{B}{N_{\sigma'}^2} \sum_{j=1}^{N_{\sigma'}} \sum_{l=1}^{N_{\sigma'}} \sin\left(2\theta_j^{\sigma'} - \theta_l^{\sigma'} - \theta_k^\sigma\right). \quad (1)$$

The indices $\sigma = 1, 2$ represent the population indices when $\sigma' = 2, 1$. Heterogeneity within a population is characterized by ω_k, which is sampled from a Lorentzian frequency distribution function $g(\omega)$ [56] with zero mean ($\omega_0 = 0$) and width $D > 0$. The parameters A and B govern the degree of pairwise and higher-order (triad) interactions, respectively. $N_{\sigma'}$ denotes the number of oscillators in the population σ'.

III. REDUCED LOW-DIMENSIONAL DYNAMICS

Now, we proceed to deduce the low-dimensional evolution equations corresponding to the macroscopic order parameters from the above discrete system of equations (1) constituting the bipartite network. In the thermodynamic limit $N_\sigma \to \infty$, the system described by Eq. (1) is reduced using the Ott-Antonsen ansatz [29]. Note that the Ott-Antonsen reduction has already been employed in bipartite networks [53,72] and in networks with higher-order interactions [68,73–77]. Let $f^\sigma(\theta : \omega, t)$ be the probability density function, representing the fraction of oscillators with phases between θ and $\theta + d\theta$ and natural frequency ω at time t. Since the number of oscillators at a given frequency ω is conserved, the dynamics of the probability density function $f^\sigma(\theta : \omega, t)$ is governed by the continuity equation

$$\frac{\partial f^\sigma}{\partial t} + \frac{\partial}{\partial \theta}(f^\sigma v^\sigma) = 0, \quad (2)$$

where $v^\sigma(\theta, t)$ represents the phase velocity, as defined in Eq. (1), which can be expressed as

$$v^\sigma(\theta, t) = \omega_k^\sigma + \frac{1}{2i}\left[H_1 e^{-i(\theta_k^\sigma)} - H_1^* e^{i(\theta_k^\sigma)} + H_2 e^{-i(\theta_k^\sigma)} - H_2^* e^{i(\theta_k^\sigma)}\right], \quad (3)$$

where the symbol $*$ represents the complex conjugate, $H_1 = A\sum_{j=1}^{N_{\sigma'}} \frac{e^{i\theta_j^{\sigma'}}}{N_{\sigma'}} = A z_1^{(\sigma')}$, and $H_2 = B\sum_{j=1}^{N_{\sigma'}} \frac{e^{i2\theta_j^{\sigma'}}}{N_{\sigma'}} \sum_{l=1}^{N_{\sigma'}} \frac{e^{-i\theta_l^{\sigma'}}}{N_{\sigma'}} = B z_2^{(\sigma')} z_1^{*(\sigma')}$. Now, using the Ott-Antonsen ansatz, the probability density function $f^\sigma(\theta : \omega, t)$ can be represented as

$$f^\sigma(\theta : \omega, t) = \frac{g(\omega)}{2\pi}\left[1 + \left(\sum_{n=1}^{\infty} a_\sigma^n(\omega, t) e^{(in\theta)} + \text{c.c.}\right)\right], \quad (4)$$

where c.c. denotes the complex conjugate. By employing Eq. (3) and Eq. (4) in Eq. (2), one can obtain the evolution equation for the Fourier coefficient $a_\sigma(\omega, t)$ as

$$\dot{a}_\sigma + i\omega a_\sigma + \frac{a_\sigma^2}{2}(H_1 + H_2) - \frac{1}{2}(H_1^* + H_2^*) = 0. \quad (5)$$

Substituting H_1 and H_2 in Eq. (5), one can obtain

$$\dot{a}_\sigma + i\omega a_\sigma + \frac{a_\sigma^2}{2}\left(A z_1^{(\sigma')} + B z_2^{(\sigma')} z_1^{*(\sigma')}\right) - \frac{1}{2}\left(A z_1^{*(\sigma')} + B z_2^{*(\sigma')} z_1^{(\sigma')}\right) = 0. \tag{6}$$

In the continuum limit, $z_1^{(\sigma)}$ can be represented as

$$z_1^{(\sigma)} = \int_{-\infty}^{\infty}\int_0^{2\pi} g(\omega) f^\sigma(\theta:\omega,t) e^{i\theta}\, d\omega\, d\theta, = \int_{-\infty}^{\infty} g(\omega) a_\sigma^*(\omega,t)\, d\omega.$$

We use the Lorentzian distribution function $g(\omega) = \frac{D/\pi}{(\omega-\omega_0)^2+D^2}$ with a mean of zero ($\omega_0 = 0$) for the frequency distribution function $g(\omega)$. This formulation allows $z_1^{(\sigma)}$ to be calculated analytically using Cauchy's residue theorem [78]. The above integral can be evaluated by closing the contour with a semicircle of infinite radius in the lower half of the complex plane and calculating the residue at the enclosed pole, which results in $z_1^{(\sigma)} = a_\sigma^*(-iD,t)$.

Similarly, $z_2^{(\sigma)}$ can be represented as

$$z_2^{(\sigma)} = \int_{-\infty}^{\infty}\int_0^{2\pi} g(\omega) f^\sigma(\theta:\omega,t) e^{i2\theta}\, d\omega\, d\theta, = \int_{-\infty}^{\infty} g(\omega) a_\sigma^{*2}(\omega,t)\, d\omega, = a_\sigma^{*2}(-iD,t), = z_1^{2(\sigma)}.$$

Using $\omega = -iD$ in Eq. (6), one can obtain the dynamics of $a_\sigma(\omega_p,t)$ from Eq. (5), which can be expressed as

$$\dot{a}_\sigma + i(-iD)a_\sigma + \frac{a_\sigma^2}{2}\left(A a_{\sigma'}^* + B a_{\sigma'}^{*2} a_{\sigma'}\right) - \frac{1}{2}\left(A a_{\sigma'} + B a_{\sigma'}^2 a_{\sigma'}^*\right) = 0. \tag{7}$$

The above equation can be represented in terms of the macroscopic parameters r_σ and ϕ_σ using $a_\sigma = r_\sigma(t)e^{-i\phi_\sigma(t)}$. Substituting $a_1 = r_1(t)e^{-i\phi_1(t)}$ and $a_2 = r_2(t)e^{-i\phi_2(t)}$ in Eq. (7), one can deduced the evolution equations for r_1, r_2, ϕ_1, and ϕ_2 as

$$\dot{r}_1 = -Dr_1 + \frac{(1-r_1^2)}{2}\left[A r_2\cos(\phi_1-\phi_2) + B r_2^3\cos(\phi_1-\phi_2)\right], \tag{8a}$$

$$\dot{r}_2 = -Dr_2 + \frac{(1-r_2^2)}{2}\left[A r_1\cos(\phi_1-\phi_2) + B r_1^3\cos(\phi_1-\phi_2)\right], \tag{8b}$$

$$\dot{\phi}_1 = -\frac{(r_1^2+1)}{2r_1}\left(A r_2\sin(\phi_1-\phi_2) + B r_2^3\sin(\phi_1-\phi_2)\right), \tag{8c}$$

$$\dot{\phi}_2 = \frac{(r_2^2+1)}{2r_2}\left(A r_1\sin(\phi_1-\phi_2) + B r_1^3\sin(\phi_1-\phi_2)\right). \tag{8d}$$

We also introduce a new parameter $\psi = \phi_1 - \phi_2$ to denote the phase difference between the populations. Consequently, the discrete system of equations (1) can be expressed in its reduced form as

$$\dot{r}_1 = -Dr_1 + \frac{(1-r_1^2)}{2}\left[A r_2\cos\psi + B r_2^3\cos\psi\right], \tag{9a}$$

$$\dot{r}_2 = -Dr_2 + \frac{(1-r_2^2)}{2}\left[A r_1\cos\psi + B r_1^3\cos\psi\right], \tag{9b}$$

$$\dot{\psi} = -\frac{(r_2^2+1)}{2r_2}\left(A r_1\sin\psi + B r_1^3\sin\psi\right) - \frac{(r_1^2+1)}{2r_1}\left(A r_2\sin\psi + B r_2^3\sin\psi\right). \tag{9c}$$

Now, the dynamics of the above system of low-dimensional evolution equations governing the macroscopic order parameters are expected to faithfully mimic the dynamics of the original discrete system of equations (1).

IV. RESULTS

Now, we will numerically solve the original discrete system of equations (1) using the Runge-Kutta fourth-order integration scheme with a step size of 0.01. We have fixed the number of oscillators in each population as $N_1 = N_2 = 2000$. The dynamics of the bipartite network (1) without the higher-order interaction are clearly disseminated by Punetha *et al.* [51], where they have clearly established that the bipartite network fails to exhibit any chimeralike state in the absence of time delay in the coupling. We have numerically calculated time-averaged order parameter $r_\sigma = \frac{1}{N}|\sum_j e^{i(\theta_j^\sigma)}|$ along with the time-averaged phase $\phi_\sigma = \arg(\frac{1}{N}\sum_j e^{i\theta_j^\sigma})$. We have depicted the absolute difference between the time-averaged order parameters $r_\sigma\,\forall\,\sigma$, defined as $\langle r\rangle = |\langle r_1\rangle - \langle r_2\rangle|$, and the difference between the time-averaged phases $\phi_\sigma\,\forall\,\sigma$, defined as $\langle\psi\rangle = |\langle\phi_1\rangle - \langle\phi_2\rangle|$, in Fig. 1 as a function of the higher-order coupling strength B. Here, the angular brackets correspond to the time average. We have fixed the width of the frequency distribution $D = 0.02$, which determines the degree of heterogeneity.

The absolute difference between the time-averaged order parameters $\langle r\rangle$ (line connected by open circles) and the difference between the time-averaged phases $\langle\psi\rangle$ (line connected by filled squares) are depicted in the left and right columns of Fig. 1, respectively. It is evident from Fig. 1(a) that $\langle r\rangle$ takes the null value in the range of $B \in [0, -0.5593]$ corroborating that both populations of the bipartite network are synchronized. We have fixed the pairwise coupling strength as $A = 0.5$. Note that the numerical order parameters r_1 and r_2 for $B = -0.25$, which quantify the degree of synchrony within the populations, become $r_1 = r_2$ asymptotically as shown in the left inset of Fig. 1(a). However, the finite value of $\langle r\rangle$ for $B < -0.5593$ elucidates that both populations evolve in asynchrony with each other. Nevertheless, the asymptotic values of the order parameters $r_1 \approx 0$ and $r_2 \approx 1$ for $B = -0.75$ [see the right inset of Fig. 1(a)] confirm that the collective state is a chimeralike state in the latter range of B. It is to be noted that we have unraveled the higher-order (triad) induced chimeralike state in a bipartite network. The difference between the

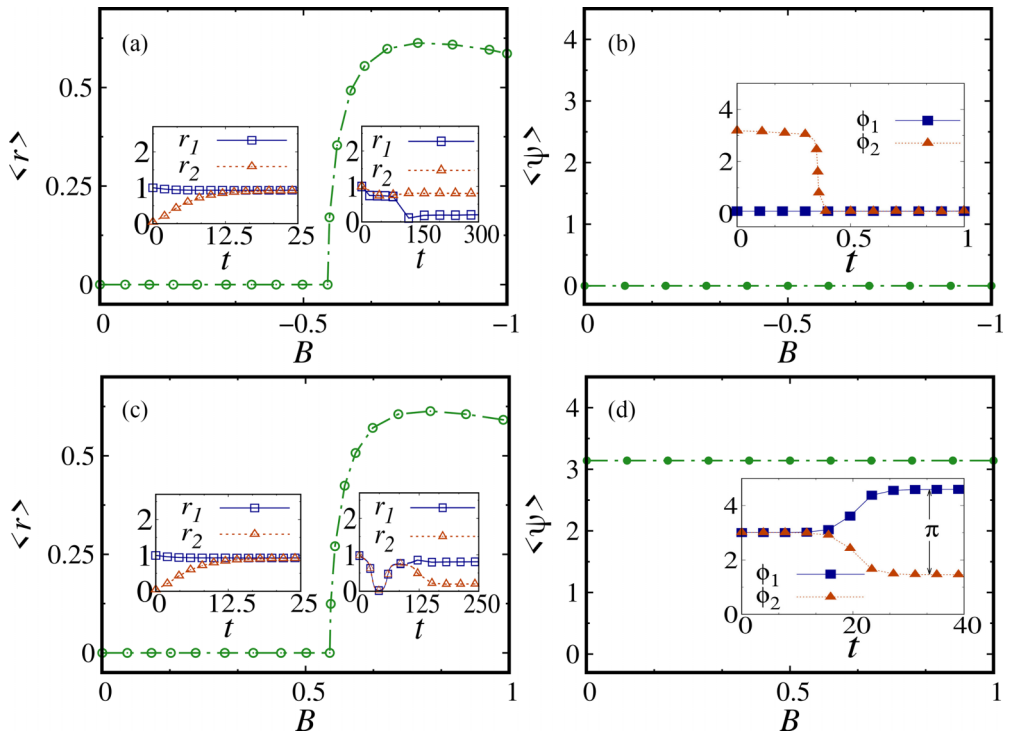

FIG. 1. Dynamical transitions as a function of higher-order (triad) interaction B. Left column: The absolute difference between the time averaged order parameters $\langle r \rangle$ (line connected by open circles). Right column: The time-averaged phase difference $\langle \psi \rangle$ (line connected by filled circles). First row: Pairwise coupling strength $A = 0.5$. Second row: Pairwise coupling strength $A = -0.5$. The order parameters r_1, and r_2, qualifying the degree of synchronization, are depicted in the inset of left column, whereas the order parameters ϕ_1 and ϕ_2, quantifying the overall phases of both populations, are depicted in the inset of right column. The width of the frequency distribution, which determines the degree of heterogeneity, is fixed as $D = 0.02$.

time-averaged phases $\langle \psi \rangle$, corresponding to Fig. 1(a), is depicted in Fig. 1(b). The null value of the time-averaged phase difference in the entire range of the higher-order coupling strength B corroborates that the two populations are in phase synchronized state characterized by $\langle \phi_1 \rangle = \langle \phi_2 \rangle$. The instantaneous phases ϕ_1 and ϕ_2 for $B = -0.25$ [see the inset of Fig. 1(b)] elucidate that both populations evolve in phase with each other.

Now, we have fixed the pairwise coupling strength as $A = -0.5$ and depicted the dynamical transitions in Figs. 1(c) and 1(d) as a function of the higher-order interaction in the range of $B \in [0, 1]$. It is clear from the figure that $\langle r \rangle = 0$ in the range of $B \in [0, 0.5593]$ corroborating that both populations evolve in synchrony. Asymptotic values of r_1 and r_2 in the left inset of Fig. 1(c) for $B = 0.25$ confirm that both populations are synchronized. However, the finite value of $\langle r \rangle$ for $B > 0.5593$ elucidates that the populations are not in synchrony in the latter range of B. Note that $r_1 \approx 1$ and $r_2 \approx 0$ asymptotically as illustrated in the right inset of Fig. 1(c) for $B = 0.75$, which indicates that the macroscopic dynamical state is a chimeralike state with coexisting synchronized population and desynchronized population of bipartite network. The time-averaged phase difference $\langle \psi \rangle$, corresponding to Fig. 1(c), is depicted in Fig. 1(d), which takes the value $\langle \psi \rangle = 3.14159$ corroborating that synchronized state is out-of-phase synchronized state in the entire explored range of B. Further, the instantaneous phases ϕ_1 and ϕ_2 for $B = 0.25$ [see the inset of Fig. 1(d)] illustrate that both populations evolve out of phase with each other. It is to be noted that when the pairwise coupling is an attractive coupling as in Fig. 1(a), the observed dynamical transitions manifest only when the higher-order interaction is a repulsive interaction and vice versa. Otherwise, only in-phase (out-of-phase) synchronized state is observed for positive (negative) values of B for attractive (repulsive) pairwise coupling, which will be evident in the two-parameter phase diagrams.

The absolute differences between the time-averaged order parameters $\langle r \rangle$ are depicted as a function of the higher-order coupling strength B in Fig. 2(a) for the pairwise coupling strength $A = 0.5$ and for different degrees of heterogeneity determined by D. The transition from synchrony to chimeralike state onsets at $B_c = -0.5593$ for $D = 0.02$ (see the line connected by unfilled circles). However, it is evident from the figure that the critical value of the higher-order coupling strength B_c required to facilitate onset of chimeralike state increases in magnitude upon increasing the degree of heterogeneity. For instance, $B_c = -0.7265$ for $D = 0.05$, $B_c = -0.8196$ for $D = 0.06$, and $B_c = -0.9478$ for $D = 0.07$. Thus, it is evident that increase in the degree of heterogeneity increases the spread of symmetric (homogeneous synchronous) state to a large range of the higher-order coupling strength among the bipartite network by decreasing the spread of symmetry-breaking (chimeralike) state. The critical value of the higher-order coupling strength B_c that breaks the symmetry among the dynamical states is shown as a function of D for three distinct values of the pairwise coupling strength in Fig. 2(b). The

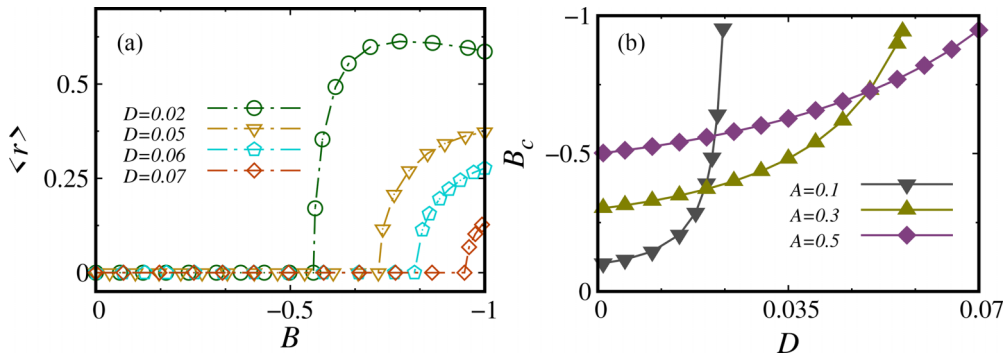

FIG. 2. Interplay between the heterogeneity and higher-order interaction. (a) Dynamical transitions as a function of higher-order coupling strength B for different degrees of heterogeneity and for $A = 0.5$, and (b) critical values of higher-order coupling strength B_c as a function of D for different degrees of pairwise coupling strength.

symmetric state prevails below (or to the right of) the curves in the (D, B_c) parameter space, whereas the symmetry-breaking state prevails above (or to the left of) the curves in the (D, B_c) parameter space. For the pairwise coupling strength $A = 0.1$, the maximum degree of heterogeneity required to break the symmetric state is $D \approx 0.023$ in the explored range of B. For $A = 0.3$, it is $D \approx 0.055$, whereas for $A = 0.5$, the maximum degree of heterogeneity increases to $D \approx 0.07$ in the explored range of B. From these results, it is evident that increase in the degree of pairwise coupling strength increases the degree of heterogeneity required to break the symmetric of the homogeneous synchronized state and consequently decreases the spread of the latter favoring the symmetry-breaking (chimeralike) state in the (D, B_c) parameter space.

One parameter bifurcation diagrams as a function of the higher-order coupling strength B for increasing degree of heterogeneity D is depicted in Fig. 3. Solid line corresponds to the stable steady states, whereas dashed dotted line corresponds to the unstable steady states that are obtained from the evolution equations for the macroscopic order parameters using the software XPPAUT [79]. Open circles connected by dotted lines are obtained directly from the numerical simulation of original discrete systems of bipartite network (1). One-parameter bifurcation diagram for the pairwise coupling strength $A = 0.5$ and $D = 0.02$ is shown in Fig. 3(a). Note that the pairwise coupling now corresponds to an attractive coupling, whereas the higher-order coupling is a repulsive coupling. The homogeneous synchronous state (SY1), characterized by the macroscopic order parameters $r_1 = r_2$, is stable in the range of $B \in [0, -0.5593]$, which loses its stability via a pitchfork bifurcation (PB) at $B = -0.5593$ resulting in the manifestation of symmetry-breaking steady (chimeralike) states, characterized by $r_1 \neq r_2$. The chimeralike state (CH1) is stable for $B < -0.5593$ as indicated by the solid (red) lines corresponding to the inhomogeneous steady states. Note that a saddle-node bifurcation (SN) at $B = -0.873939$ has resulted in a homogeneous stable steady state, which corresponds to the second synchronized state indicated by SY2. SY1 is characterized by the macroscopic order parameter $\psi = 0$ elucidating that the synchronized state SY1 is an in-phase synchronized state in concurrence with the numerical order parameters depicted in Figs. 1(a) and 1(b). Similarly, SY2 is characterized by the macroscopic order parameter $\psi = \pi$ corroborating that the synchronized state SY2 is an out-of-phase synchronized state as observed numerically in Figs. 1(c) and 1(d). It is also to be noted that CH1 and SY2 states coexist for $B < -0.873939$ leading to the emergence of bistable states.

A bifurcation diagram similar to Fig. 3(a) is observed in Fig. 3(b) for $A = -0.5$ and $D = 0.02$. Note that the pairwise coupling now corresponds to a repulsive coupling, whereas higher-order coupling is an attractive coupling. Now, out-of-phase synchronized state (SY2) is observed in the range $B \in [0, 0.5593]$, which loses its stability via a pitchfork bifurcation resulting in the symmetry-breaking chimeralike state (CH2), which is stable for $B > 0.5593$. The in-phase synchronized state (SY1) manifests via a saddle-node bifurcation at $B = 0.873939$. It is to be noted that the symmetry-breaking chimeralike state (CH2) manifests from the out-of-phase synchronized state (SY2), which coexists with the SY1 state in the range $B \in [0.8739, 1]$. In contrast, in Fig. 3(a), the chimeralike state (CH1) manifested from the destabilization of the in-phase synchronized state. Now, one-parameter bifurcation diagram for $A = 0.5$ and increased degree of heterogeneity $D = 0.05$ is illustrated in Fig. 3(c). The out-of-phase synchronized state (SY2) loses its stability and completely whipped off from the bifurcation diagram, while the range of stable homogeneous in-phase synchronous state is increased with decrease in the spread of chimeralike (CH1) state as observed in Fig. 2(a). Further increase in the degree of heterogeneity to $D = 0.07$, for the same pairwise coupling strength, the spread of the symmetric in-phase synchronous state is increased further [see Fig. 3(d)] as observed in Fig. 2(a) for $D = 0.07$ at the expense of the spread of the symmetry-breaking chimeralike state (CH1). Thus, the increased degree of heterogeneity promotes the symmetric homogeneous in-phase synchronized state. Similar results are also observed as a function of attractive higher-order coupling strength for the repulsive pairwise coupling strength, where the symmetric homogeneous state, characterized by $r_1 = r_2$, is an out-of-phase synchronized state (SY2).

One-parameter bifurcation diagrams, obtained both from the evolution equation for the macroscopic variables (9) and from the original discrete model (1), are plotted in Fig. 4 as a function of the pairwise coupling strength A for two different D. The higher-order coupling strength is fixed as $B = -0.948$.

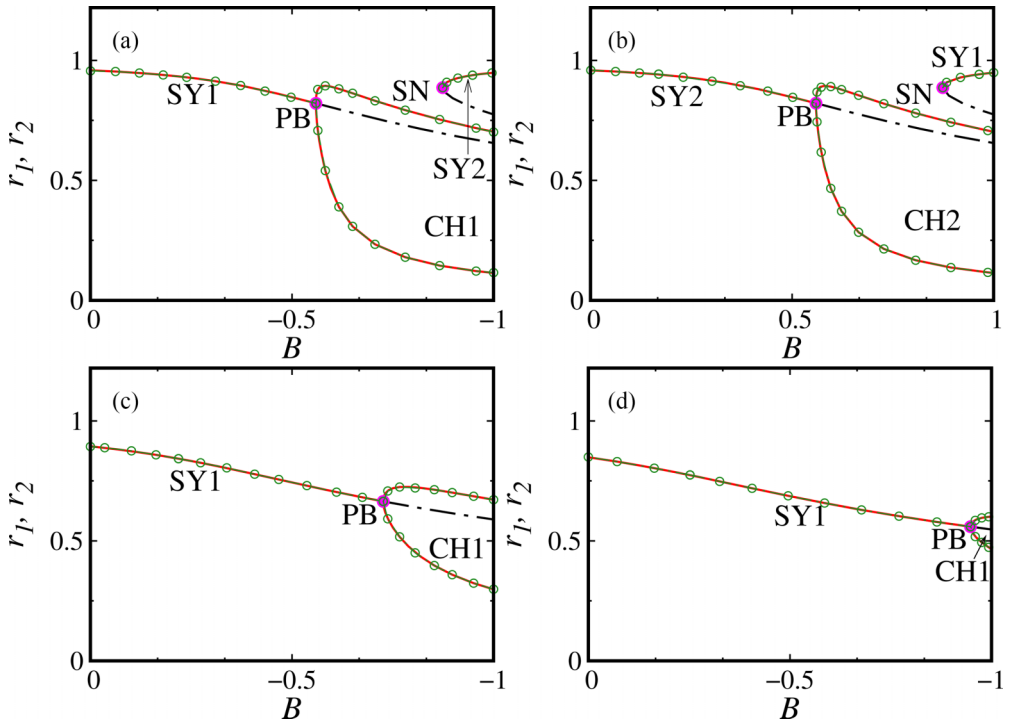

FIG. 3. One-parameter bifurcation diagrams as a function of the higher-order coupling strength B for increasing degree of heterogeneity D. (a) and (b) $D = 0.02$, (c) $D = 0.05$, and (d) $D = 0.07$. The pairwise coupling strength is $A = -0.5$ in (b) and 0.5 in all other subfigures. Solid line corresponds to the stable steady states, whereas dashed dotted line corresponds to the unstable steady state that are obtained from the evolution equations (9) for the macroscopic order parameters using the software XPPAUT. Open circles connected by dotted lines are obtained directly from the numerical simulation of original discrete systems of bipartite network (1). PB corresponds to the pitchfork bifurcation, while SN corresponds to the saddle-note bifurcation.

The dynamical states, their transitions and involved bifurcations are the same as in Fig. 3. Note that here incoherent state in the range of $A \in [0, 0.033)$ coexists with the SY2, the latter of which loses its stability via a SN bifurcation at $A = 0.5585$ [see Fig. 4(a) for $D = 0.02$]. SY1 coexists with SY2 in the range of $A \in [0.033, 0.0859]$ and then loses its stability via a PB bifurcation leading to the manifestation of symmetry-breaking state (CH1). Note that CH1 coexists with SY2 in the range of $A \in (0.0859, 0.8956]$, which loses its stability via a second PB bifurcation at $A = 0.8956$ resulting in the reemergence of SY1 state. Similar dynamical transitions are observed for increased degree of heterogeneity in Fig. 4(b) for $D = 0.05$. Note that the range of incoherence state, SY1 state are increased with decrease in the spread of SY2 and CH1 states, thereby corroborating that increased heterogeneity facilitates the homogeneous (symmetric in-phase) states to a large range of the parameters as observed in Fig. 2(a) and Fig. 4.

Next, we have depicted the two-parameter phase diagrams in the (B, A) parameter space in Fig. 5 for two different D for a global perspective of the observed dynamical states, their bistability, dynamical transitions, and accompanied bifurcation curves. The homogeneous SY1 and SY2 states are indicated by yellow shaded region and region with brown diagonal lines, respectively. The inhomogeneous CH1 and CH2 states are represented by the green shaded region and

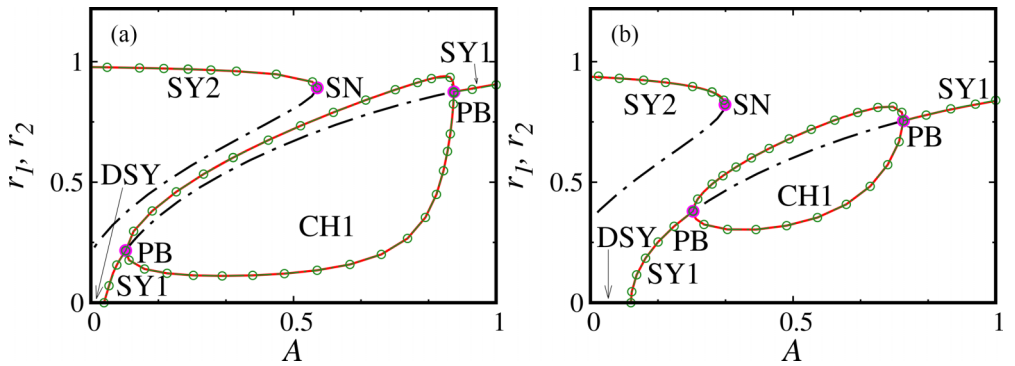

FIG. 4. One-parameter bifurcation diagrams as a function of the pairwise coupling strength A for increasing degree of heterogeneity D. The higher-order coupling strength is fixed as $B = -0.948$. (a) $D = 0.02$, and (b) $D = 0.05$. The other details are the same as in Fig. 3.

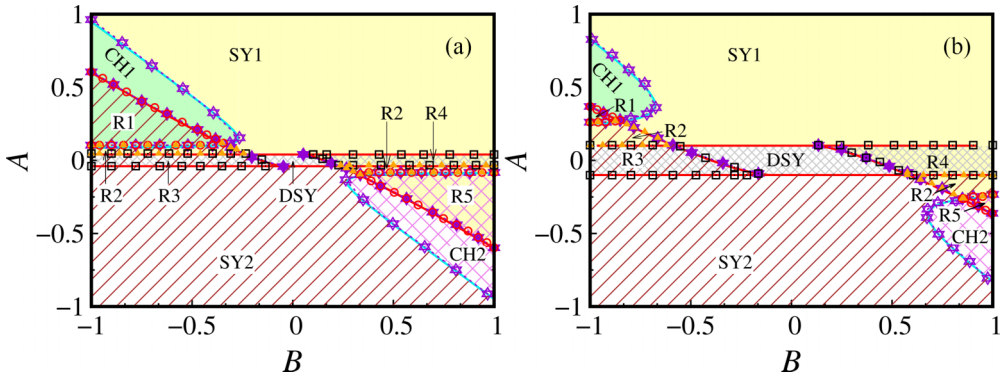

FIG. 5. Two-parameter phase diagrams in the (B, A) parameter space for different degrees of heterogeneity. (a) $D = 0.02$, and (b) $D = 0.05$. Refer text for more details.

pink checked region, respectively. Incoherent state (DSY) is indicated by a light gray checked region between the parallel horizontal red lines about $A = 0$. The bistability between CH1 and SY2, denoted by the region R1, is enclosed by a line connecting open circles. The bistability between SY1 and SY2, denoted by the region R2, is enclosed by a line connecting filled triangles. The bistability between DSY and SY2, denoted by the region R3, is enclosed by a line connecting black open squares. Similarly, the bistability between DSY and SY1, denoted by the region R4, is enclosed by a line connecting open squares. The bistability between CH2 and SY1, denoted by the region R5, is enclosed by a line connecting open circles. The dynamical states and their transitions in the phase diagrams are the same as observed in the one-parameter bifurcation diagrams. In particular, for $B = -0.948$ [see Fig. 5(a) for $D = 0.02$], one can observe the dynamical transition discussed in Fig. 4(a) in the range of $A \in [0, 1]$. Similarly, for $A = 0.5$, one can observe the dynamical transition demonstrated in Fig. 3(a) in the range of $B \in [-1, 0]$ and for $A = -0.5$, one can observe the dynamical transition in Fig. 3(b) in the range of $B \in [0, 1]$. Note that when the pairwise coupling is an attractive coupling, the observed dynamical transitions manifest only when the higher-order interaction is repulsive in nature and vice versa. Otherwise, it is evident that only in-phase (out-of-phase) synchronized state is observed for positive (negative) values of B for attractive (repulsive) pairwise coupling as pointed out above while explaining Fig. 1.

The solid (cyan) line, corresponding to the pitchfork bifurcation curve, encompassing CH1 (CH2) state across which SY1(SY2) loses stability is obtained from the evolution equations for the macroscopic order parameters using the XPPAUT software. Similarly, the slanting (red) lines, corresponding to the saddle-node bifurcation curve, across which SY2 loses its stability in the range of $B \in [-1, 0]$ and SY1 loses its stability in the range of $B \in [0, 1]$ in Fig. 5(a) are also obtained using the XPPAUT software. The shaded regions are obtained by numerically solving the discrete model (1). Note that the XPPAUT bifurcation curves exactly match the simulation boundaries. A similar phase diagram is observed in Fig. 5(b) for $D = 0.05$, where the spread of homogeneous synchronized states are increased due to increased heterogeneity at the cost of the spread of symmetry-breaking chimeralike states. Now, one can deduce the analytical stability condition across which the in-phase (SY1) and out-of-phase synchronized (SY2) state lose their stability using a linear stability analysis of the evolution equations for the macroscopic order parameters about appropriate fixed points. To identify the in-phase synchronized region, set $r_1 = r_2 = r$ and $\psi = 0$ in Eqs. (9a) and (9b). The fixed points can be obtained, by solving the resulting evolution equations for the macroscopic order parameters, as

$$r^2 = \frac{B - A + \sqrt{(A+B)^2 - 8BD}}{2B}. \tag{10}$$

A linear stability analysis of Eqs. (9) around the fixed point $r_1 = r_2 = r$ and $\psi = 0$ yields a characteristic equation. Using one of the Routh-Hurwitz stability criterion, namely $\det(J) = 0$, where J represents the Jacobian of (9), one can obtain the stability condition for the fixed point as an algebraic expression involving A, B, and D as

$$\begin{aligned}\sqrt{(A+B)^2 - 8BD}(A^2B + A^3 + AB^2 - 6ABD - 2B^2D \\ +B^3) + 10A^2BD - 2A^3B - A^4 + 4AB^2D \\ +2AB^3 - 16B^2D^2 - 6B^3D + B^4 = 0.\end{aligned} \tag{11}$$

One can get five distinct solutions upon solving the above equation for B. Two among the solutions turn out to be the stability condition for the in-phase synchronized state in the (B, A) parameter space. One corresponds to the pitchfork bifurcation curve, which is depicted as a line connecting open stars in Fig. 5 in the range of $B \in [-1, 0]$, while the other corresponds to the saddle-node bifurcation curve, which is depicted as a line connecting filled stars in Fig. 5 in the range of $B \in [0, 1]$. The stability condition for the out-of-phase synchronized state is obtained by setting $r_1 = r_2 = r$ and $\psi = \pi$ in Eqs. (9a) and (9b). Now, one can deduce the fixed points, by imposing the above conditions on the macroscopic order parameters, as

$$r^2 = \frac{B - A - \sqrt{(A+B)^2 + 8BD}}{2B}. \tag{12}$$

As mentioned above, a linear stability analysis of Eqs. (9) about these fixed points, using the Routh-Hurwitz stability criterion [$\det(J) = 0$], results in the algebraic expression involving A, B, and D represented as

$$\begin{aligned}\sqrt{(A+B)^2 + 8BD}(A^2B + A^3 + AB^2 + 6ABD + 2B^2D \\ +B^3) + 10A^2BD + 2A^3B + A^4 + 4AB^2D \\ -2AB^3 + 16B^2D^2 - 6B^3D - B^4 = 0.\end{aligned} \tag{13}$$

Again, one can get five distinct solutions upon solving the above equation for B. Two among the solutions turn out to be the stability condition for the out-of-phase synchronized state in the (B, A) parameter space. One corresponds to the pitchfork bifurcation curve, which is depicted as a line connecting open stars in Fig. 5 in the range of $B \in [0, 1]$, while the other corresponds to the saddle-node bifurcation curve, which is depicted as a line connecting filled stars in Fig. 5 in the range of $B \in [-1, 0]$.

It is also possible to deduce the stability condition for the desynchronized state by performing a linear stability analysis about the fixed points $r_1 = r_2 = 0$ and $\psi = 0$. Imposing $\psi = 0$ in Eqs. (9a) and (9b) results in

$$\dot{r}_1 = -Dr_1 + 0.5\left(1 - r_1^2\right)\left(A\, r_2 + B\, r_2^3\right), \tag{14a}$$

$$\dot{r}_2 = -Dr_2 + 0.5\left(1 - r_2^2\right)\left(A\, r_1 + B\, r_1^3\right). \tag{14b}$$

A linear stability analysis of the above evolution equations for r_1 and r_2 about the fixed point $r_1 = r_2 = 0$ yields the eigenvalues

$$\lambda = \frac{-2D \pm A}{2}, \tag{15}$$

which leads to the condition for the stability of the desynchronized state, by setting $\lambda = 0$, as

$$A = \pm 2D. \tag{16}$$

Now, substituting $D = 0.02 (D = 0.05)$ into Eq. (16), we find that the desynchronized region is bounded by $A = \pm 0.04 (A = \pm 0.1)$. This analytical condition perfectly aligns with the numerical and XPPAUT boundaries encompassing the stable region of desynchronized state, represented by the two horizontal parallel red lines, in [Figs. 5(a) and 5(b)]. It is also to be noted that all the deduced analytical stability curves match exactly with the simulation boundaries and XPPAUT bifurcation curves.

V. CONCLUSION

We have considered a bipartite network of phase oscillators with both pairwise and higher-order interactions. We have elucidated that the higher-order interaction facilitates the manifestation of stable chimeralike state in the bipartite network of phase oscillators by breaking the symmetry of the homogeneous synchronized states. In particular, we have demonstrated that the bipartite network exhibits a transition from in-phase synchronized (symmetric) state to symmetry-breaking chimeralike state as a function of repulsive higher-order interaction when the pairwise interaction is an attractive coupling. In contrast, we have shown that the bipartite network exhibits transition from out-of-phase synchronized (symmetric) state to symmetry-breaking chimeralike state as a function of attractive higher-order interaction when the pairwise interaction is a repulsive coupling. We have also illustrated that only in-phase (out-of-phase) synchronized state is observed for attractive (repulsive) higher-order interaction for attractive (repulsive) pairwise coupling using the two-parameter phase diagrams. Increasing the degree of heterogeneity of the phase oscillators using the Lorentzian distribution function $g(\omega)$, we found that the symmetric homogeneous synchronized states are stabilized to a large region of the parameter space by destabilizing the symmetry-breaking chimeralike states, elucidating heterogeneity promotes homogeneity [80]. We have also shown that increase in the degree of pairwise coupling strength increases the degree of heterogeneity required to break the symmetric state and consequently decreases the spread of the latter favoring the symmetry-breaking (chimeralike) state in the (D, B_c) parameter space.

We have also deduced the low-dimensional evolution equations corresponding to the macroscopic order parameters from the original discrete system of bipartite network using the Ott-Antonsen ansatz. We have demonstrated that both in-phase and out-of-phase synchronized states lose their stability via a pitchfork bifurcation curve resulting in two distinct chimeralike states. Further, we have shown that a saddle-node bifurcation results in the manifestation of symmetric synchronized states, which coexist with the symmetry-breaking chimeralike state. The bifurcation curves obtained from the evolution equations for the macroscopic order parameters using XPPAUT are found to match very well with the simulation results. Furthermore, we have analytically deduced the stability conditions for the incoherence state, in-phase, and out-of-phase synchronized states using a linear stability analysis of the evolution equations for the macroscopic order parameters, which are found to agree with the bifurcation curves obtained using XPPAUT. We strongly believe that the current results will enhance our understanding of the onset of chimera and chimeralike state in an important class of complex network, namely bipartite network, and will create new avenues to identify its potential application in such a network.

ACKNOWLEDGMENTS

R.K. acknowledges IISER-TVM for infrastructural and funding support. The work of V.K.C. is supported by the DST-CRG Project under Grant No. CRG/2020/004353 and DST, New Delhi for computational facilities under the DST-FIST program (SR/FST/PS- 1/2020/135) to the Department of Physics. D.V.S. is supported by the DST-CRG Project under Grant No. CRG/2021/000816.

[1] Y. Kuramoto and D. Battogtokh, Nonlinear Phenom. Complex Syst. **5**, 380 (2002).
[2] C. R. Laing, Phys. Rev. E **92**, 050904(R) (2015).
[3] V. García-Morales, J. A. Manzanares, and K. Krischer, Chaos, Solitons Fractals **165**, 112808 (2022).
[4] L. Schmidt and K. Krischer, Chaos **25**, 064401 (2015).
[5] J. Singha and N. Gupte, Phys. Lett. A **384**, 126225 (2020).
[6] S. Saha and S. K. Dana, Chaos **33**, 092101 (2023).
[7] M. R. Tinsley, S. Nkomo, and K. Showalter, Nature Phys. **8**, 662 (2012).

[8] K. Schönleber, C. Zensen, A. Heinrich, and K. Krischer, New J. Phys. **16**, 063024 (2014).

[9] S. Nkomo, M. R. Tinsley, and K. Showalter, Phys. Rev. Lett. **110**, 244102 (2013).

[10] S. Nkomo, M. R. Tinsley, and K. Showalter, Chaos **26**, 094826 (2016).

[11] J. Shena, J. Hizanidis, V. Kovanis, and G. P. Tsironis, Sci. Rep. **7**, 42116 (2017).

[12] F. Böhm, A. Zakharova, E. Schöll, and K. Lüdge, Phys. Rev. E **91**, 040901(R) (2015).

[13] E. A. Martens, S. Thutupalli, A. Fourriére, and O. Hallatschek, Proc. Natl. Acad. Sci. **110**, 10563 (2013).

[14] H. Yin, Am. J. Phys. Appl. **7**, 27 (2019).

[15] T. Bountis, V. G. Kanas, J. Hizanidis, and A. Bezerianos, Eur. Phys. J. Spec. Top. **223**, 721 (2014).

[16] L. V. Gambuzza, A. Buscarino, S. Chessari, L. Fortuna, R. Meucci, and M. Frasca, Phys. Rev. E **90**, 032905 (2014).

[17] B. K. Bera, D. Ghosh, and M. Lakshmanan, Phys. Rev. E **93**, 012205 (2016).

[18] L. Khaleghi, S. Panahi, S. N. Chowdhury, S. Bogomolov, D. Ghosh, and S. Jafari, Physica A **536**, 122596 (2019).

[19] I. A. Shepelev, T. E. Vadivasova, A. Bukh, G. Strelkova, and V. Anishchenko, Phys. Lett. A **381**, 1398 (2017).

[20] S. Majhi, M. Perc, and D. Ghosh, Sci. Rep. **6**, 39033 (2016).

[21] A. V. Andreev, M. V. Ivanchenko, A. N. Pisarchik, and A. E. Hramov, Chaos, Solitons Fractals **139**, 110061 (2020).

[22] M. Shafiei, S. Jafari, F. Parastesh, M. Ozer, T. Kapitaniak, and M. Perc, Commun. Nonlinear Sci. Numer. Simul. **84**, 105175 (2020).

[23] J. Khouhak, Z. Faghani, J. L. Laugesen, and S. Jafari, Chin. J. Phys. **63**, 402 (2020).

[24] L. Bauer, J. Bassett, P. Hóvel, Y. N. Kyrychko, and K. B. Blyuss, Chaos **27**, 114317 (2017).

[25] Z. Shahriari, F. Parastesh, M. Jalili, V. Berec, J. Ma, and S. Jafari, Europhys. Lett. **125**, 60001 (2019).

[26] O. E. Omel'chenko, Nonlinearity **31**, R121 (2018).

[27] P. Clusella and A. Politi, Phys. Rev. E **99**, 062201 (2019).

[28] M. J. Panaggio, D. M. Abrams, P. Ashwin, and C. R. Laing, Phys. Rev. E **93**, 012218 (2016).

[29] M. J. Panaggio and D. M. Abrams, Nonlinearity **28**, R67(R) (2015); Phys. Rev. E **91**, 022909 (2015).

[30] A. M. Hagerstrom, T. E. Murphy, R. Roy, P. Hövel, I. Omelchenko, and E. Schöll, Nature Phys. **8**, 658 (2012).

[31] J. D. Hart, K. Bansal, T. E. Murphy, and R. Roy, Chaos **26**, 094801 (2016).

[32] D. M. Abrams and S. H. Strogatz, Phys. Rev. Lett. **93**, 174102 (2004).

[33] S. Majhi, B. K. Bera, D. Ghosh, and M. Perc, Phys. Life Rev. **28**, 100 (2019).

[34] N. Lotfi and A. H. Darooneh, Int. J. Mod. Phys. C **31**, 2050069 (2020).

[35] S. Ghosh and S. Jalan, Int. J. Bifurcation Chaos **26**, 1650120 (2016).

[36] F. Parastesh, C.-Y. Chen, H. Azarnoush, S. Jafari, and B. Hatef, Eur. Phys. J. Spec. Top. **228**, 2465 (2019).

[37] M. Goremyko, V. Maksimenko, V. Makarov, D. Ghosh, B. Bera, S. Dana, and A. Hramov, Tech. Phys. Lett. **43**, 712 (2017).

[38] X. Li, T. Xu, and J. Li, Eur. Phys. J. Spec. Top. **228**, 2419 (2019).

[39] O. E. Omel'chenko, M. Wolfrum, S. Yanchuk, Y. L. Maistrenko, and O. Sudakov, Phys. Rev. E **85**, 036210 (2012).

[40] L. Kang, C. Tian, S. Huo, and Z. Liu, Sci. Rep. **9**, 1 (2019).

[41] Y. Liu, A. J. M. Khalaf, S. Jafari, and I. Hussain, Europhys. Lett. **127**, 40001 (2019).

[42] V. Maistrenko, O. Sudakov, and O. Osiv, Chaos **30**, 063113 (2020).

[43] S. Kundu, B. K. Bera, D. Ghosh, and M. Lakshmanan, Phys. Rev. E **99**, 022204 (2019).

[44] C. Tian, H. Bi, X. Zhang, S. Guan, and Z. Liu, Phys. Rev. E **96**, 052209 (2017).

[45] E. A. Martens, Chaos **20**, 043122 (2010).

[46] T. Njougouo, G. R. Simo, P. Louodop, H. Fotsin, and P. K. Talla, Chaos, Solitons Fractals **139**, 110082 (2020).

[47] W.-H. Wang, Q.-L. Dai, H.-Y. Cheng, H.-H. Li, and J.-Z. Yang, Front. Phys. **14**, 43605 (2019).

[48] Y. Li, A. Wen, Q. Lin, R. Li, and L. Zhengding, Artif. Intell. Rev. **41**, 563 (2014).

[49] D. Coates, I. Naidenova, and P. Parshakov, Int. J. Sport Fin. **15**, 95 (2020).

[50] C. Villiers, *The Role of Investor Networks in Transnational Corporate Governance, Networked Governance* (Springer, Berlin, 2014), p. 285.

[51] N. Punetha, S. R. Ujjwal, F. M. Atay, and R. Ramaswamy, Phys. Rev. E **91**, 022922 (2015).

[52] Z. M. Wu, H. Y. Cheng, Y. Feng, H. H. Li, Q. L. Dai, and J. Z. Yang, Front. Phys. **13**, 130503 (2018).

[53] Q. Dai, Q. Liu, H. Cheng, H. Li, and J. Yang, Nonlinear Dyn. **92**, 741 (2018).

[54] I. Omelchenko, Y. Maistrenko, P. Hovel, and E. Schöll, Phys. Rev. Lett. **106**, 234102 (2011).

[55] C. R. Laing, K. Rajendran, and I. G. Kevrekidis, Chaos **22**, 013132 (2012).

[56] T. Kotwal, X. Jiang, and D. M. Abrams, Phys. Rev. Lett. **119**, 264101 (2017).

[57] E. A. Martens, C. Bick, and M. J. Panaggio, Chaos **26**, 094819 (2016).

[58] S. Rakshit, B. K. Bera, M. Perc, and D. Ghosh, Sci. Rep. **7**, 2412 (2017).

[59] E. A. Martens, M. J. Panaggio, and D. M. Abrams, New J. Phys. **18**, 022002 (2016).

[60] S. Boccaletti, P. D. Lellis, C. I. del Genio, K. A. Bittner, R. Criado, S. Jalan, and M. Romance, Phys. Rep. **1018**, 1 (2023).

[61] A. Patania, G. Petri, and F. Vaccarino, EPJ Data Sci. **6**, 18 (2017).

[62] A. E. Sizemore, C. Giusti, A. Kahn, J. M. Vettel, R. F. Betzel, and D. S. Bassett, J. Comp. Neurosci. **44**, 115 (2018).

[63] G. Petri, P. Expert, F. Turkheimer, R. Carhart-Harris, D. Nutt, P. J. Hellyer, and F. Vaccarino, J. R. Soc. Interface **11**, 20140873 (2014).

[64] E. Estrada and G. J. Ross, J. Theor. Biol. **438**, 46 (2018).

[65] A. P. Millan, J. J. Torres, and G. Bianconi, Phys. Rev. Lett. **124**, 218301 (2020).

[66] P. S. Skardal and A. Arenas, Phys. Rev. Lett. **122**, 248301 (2019).

[67] D. M. Abrams, R. Mirollo, S. H. Strogatz, and D. A. Wiley, Phys. Rev. Lett. **101**, 084103 (2008).

[68] S. Kundu and D. Ghosh, Phys. Rev. E **105**, L042202 (2022).
[69] X. Li, D. Gosh, and Y. Lei, Chaos, Solitons Fractals **170**, 113325 (2023).
[70] C. Bick, Phys. Rev. E **97**, 050201(R) (2018).
[71] C. Bick, J. Nonlin. Sci. **29**, 2547 (2019).
[72] J. Singha and R. Ramaswamy, Chaos, Solitons Fractals **157**, 111947 (2022).
[73] P. S. Skardal and A. Arenas, Commun. Phys. **3**, 218 (2020).
[74] A. D. Kachhvah and S. Jalan, Phys. Rev. E **105**, L062203 (2022).
[75] R. Kar, A. Yadav, V. K. Chandrasekar, and D. V. Senthilkumar, Chaos **34**, 023110 (2024).
[76] M. Manoranjani, R. Gopal, D. V. Senthilkumar, V. K. Chandrasekar, and M. Lakshmanan, Phys. Rev. E **105**, 034307 (2022).
[77] S. Dutta, A. Mondal, P. Kundu, P. Khanra, P. Pal, and C. Hens, Phys. Rev. E **108**, 034208 (2023).
[78] M. J. Ablowitz and A. S. Fokas, *Complex Variables: Introduction and Applications* (Cambridge University Press, Cambridge, England, 2003).
[79] B. Ermentrout, *Simulating, Analyzing, and Animating Dynamical Systems: A Guide to XPPAUT for Researchers and Students*, (Society for Industrial & Applied Math, Philadelphia, 2002).
[80] Y. Zhang, J. L. Ocampo-Espindola, I. Z. Kiss, and A. E. Motter, Proc. Natl. Acad. Sci. USA **118**, e2024299118 (2021).